

Iso-Diffusion: Improving Diffusion Probabilistic Models Using the Isotropy of the Additive Gaussian Noise

Dilum Fernando
Johns Hopkins University
Baltimore, USA
bferna12@jh.edu

H.L.P. Malshan
University of Peradeniya
Peradeniya, Sri Lanka
e17205@eng.pdn.ac.lk

H.M.V.R. Herath
University of Peradeniya
Peradeniya, Sri Lanka
vijitha@eng.pdn.ac.lk

Shakthi Perera
University of Peradeniya
Peradeniya, Sri Lanka
e17245@eng.pdn.ac.lk

Roshan Godaliyadda
University of Peradeniya
Peradeniya, Sri Lanka
roshangodd@ee.pdn.ac.lk

Dhananjaya Jayasundara
Johns Hopkins University
Baltimore, USA
vjayasul@jh.edu

H.M.P.S. Madushan
University of Peradeniya
Peradeniya, Sri Lanka
pathumshehara@eng.pdn.ac.lk

M.P.B. Ekanayake
University of Peradeniya
Peradeniya, Sri Lanka
mpb.ekanayake@ee.pdn.ac.lk

Chaminda Bandara
Apple Inc.
Seattle, USA
c.bandara@apple.com

Abstract

Denoising Diffusion Probabilistic Models (DDPMs) have accomplished much in the realm of generative AI. With the tremendous level of popularity the Generative AI algorithms have achieved, the demand for higher levels of performance continues to increase. Under this backdrop, careful scrutiny of algorithm performance under sample fidelity type measures is essential to ascertain how, effectively, the underlying structures of the data distribution were learned. In this context, minimizing the mean squared error between the additive and predicted noise alone does not impose structural integrity constraints on the predicted noise, for instance, isotropic. Under this premise, we were motivated to utilize the isotropy of the additive noise as a constraint on the objective function to enhance the fidelity of DDPMs. Our approach is simple and can be applied to any DDPM variant. We validate our approach by presenting experiments conducted on four synthetic 2D datasets as well as on unconditional image generation. As demonstrated by the results, the incorporation of this constraint improves the fidelity metrics, Precision and Density, and the results clearly indicate how the structural imposition was effective.

1. Introduction

Diffusion models have been accomplishing great feats in the realm of generative AI, specifically in terms of uncon-

ditional and conditional image generation ([19], [9], [26], [18], [22], [24], [6], [10], [1]). Starting with the revolutionary paper by Ho et al. [7] and the improvements by Nichol et al. [19] as well as the Latent Diffusion Model by Rombach et al. [24], these models have had the biggest impact in this context. The fidelity and diversity of the images generated by these models are surprisingly amazing. Yet, as with all models, these models can still be improved upon closer inspection. As with the improvements done by Nichol et al. [19] to the original Denoising Diffusion Probabilistic Model (DDPM) by introducing techniques such as the cosine-based variance schedule and allowing the model to learn the variance rather than keeping it fixed helped improve the performance of DDPMs. Our goal in this paper is to make a similar contribution with regard to the improvement of the important fidelity metrics, Density [16] and Precision [13], by imposing possible regularizations that promote the modified DDPM algorithm to learn the underlying structures, diversity, modality and density spread of the true distribution.

Although DDPMs perform well, we noticed that these existing models do not necessarily incorporate any distributional (structural) information about the particular dataset it tries to generate. Typically, the DDPM’s forward process gradually pushes the dataset towards an isotropic Gaussian, which can be thought of as the structural vanishing point of the data distribution [17]. This implies a well-placed point of origin for the generative process (reverse

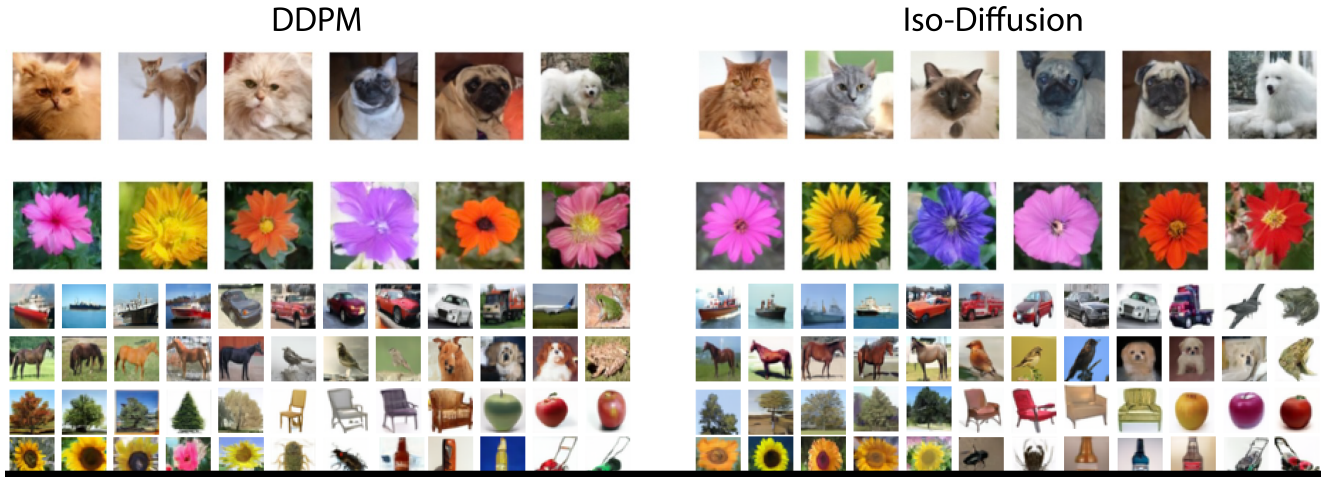


Figure 1. Comparison of the generated images via the DDPM (left) and Iso-Diffusion (right). The DDPM generated images contain much more artefacts and do not seem realistic. However, the generated images via Iso-Diffusion are much more realistic and thus, they are of high fidelity.

path) from a point of complete lack of structure toward the final destination, which is the data distribution. In the DDPM implementation, the learning process considers the expected squared norm difference between the additive Gaussian noise and the predicted noise as its objective function. Therefore, for the generative process, to enhance the aforementioned creation of structure, the objective function can be modified to include any structural measure, such as isotropy.

Thus, we were motivated to include the isotropic nature of the additive Gaussian noise when optimizing for the objective to further enhance the statistical properties of the predicted noise through backpropagation. The current objective function of the DDPM does not include any mechanism that explicitly encourages the isotropic nature of the predicted noise. Therefore, a mechanism that guarantees the model progresses from a more non-isotropic distribution (distributions with multiple modes, discontinuities or non-uniformities of density distributions, non-uniformly distributed spatial structures) to an isotropic Gaussian distribution toward the vanishing point in a structured and learned manner is needed. Our intuition is that by capturing the statistical properties of the noise in more detail, the model will be able to produce higher-fidelity samples as it would have much more information regarding the distributional structure of the samples.

As the rationale for introducing isotropy to the objective function has been established, now, let us see how isotropy establishes convergence and quantifies structural information about the distribution. For example, the isotropy of an isotropic random vector in \mathbb{R}^n is the expected squared norm of that vector, which is equal to its dimension, n [34]. This establishes the convergence in the limit for a normal-

ized distribution with a complete lack of structure, which in other words is isotropic. Conversely, the desired distribution, which has more structure and is more non-isotropic, would consequently have a lower isotropy value. This implies that the generative process, in its drive towards a structural distribution, minimizes isotropy. Furthermore, when analyzing the mean square error objective, we observed that incorporating the isotropic nature of the noise effectively makes the objective function equal to zero in expectation.

The inclusion of this constraint does not incur a large computational cost and can be readily applied to any of the diffusion model variants. In this work, we scrutinized the DDPM model’s behavioral aspects to interpret its functionality using well-defined 2D synthetic datasets, such as Swiss Roll, Scattered Moon, Moon with two circles and Central Banana, to draw fundamental conclusions about DDPM algorithm. Furthermore, we experimented on four 2D synthetic datasets with our modified objective function and showed that the fidelity metrics, in particular the Precision and Density, improved significantly. In addition, we validate our approach to unconditional image generation using the Oxford Flower [20] and Oxford-IIIT Pet [21], CIFAR-10 [12] and CIFAR-100 [12] datasets. We compare the fidelity and diversity of the generated samples based on key evaluation metrics such as Precision and Recall [13], Density and Coverage [16], Frechet Inception Distance (FID) [5] and Inception Score (IS) [28].

The contributions of this work are as follows:

- We introduce Iso-Diffusion: a modified approach that introduces an isotropic constraint on the predicted noise objective function to steer the generative process in a structurally coherent manner. This results in improved fidelity of the generated data distribution. We believe, to the best

of our knowledge, that we are the first to propose such a modified loss based on the structural properties of the noise.

- We analyze the simple loss function in the DDPM and its connection to isotropy. Moreover, we show that the isotropy of the data distribution monotonically increases and converges to the maximum isotropy value, which corresponds to an isotropic Gaussian distribution. This confirms that the definition of isotropy mentioned in this paper, conveys information about the structure of the data distribution when the data distribution undergoes the forward process in DDPMs.
- We evaluate and validate our approach on four 2D synthetic datasets as well as on the task of unconditional image generation on Oxford Flower, Oxford-IIIT Pet, CIFAR-10 and CIFAR-100 datasets. Considering the key evaluation metrics, such as Precision, Recall, Density, Coverage, FID and IS, the modified objective is able to surpass the original DDPM with a significant gap in terms of the fidelity metrics, Density and Precision.
- We conduct an in-depth analysis of the Density and Coverage metrics to evaluate the generative capabilities of Iso-Diffusion compared to DDPM. This analysis facilitates a detailed comparison between the generated and true data distributions, visually illustrating Iso-Diffusion’s superior alignment with the true distribution. Furthermore, it highlights the importance of these metrics for assessing generative AI algorithms in computer vision applications.

2. Related Work

Generative models, particularly in recent years, have gained significant momentum due to their applications in various fields. They began with specific use cases and have evolved along a clear trajectory, as outlined below.

Deep Generative Models Generative models (GANs [3], VAEs [11], flow-based models [23], and diffusion models [7]) learn the probability distribution of given data, allowing us to sample new data points from the distribution. Deep generative models have been used for generating images, videos [8], 3d objects [15], etc. Moreover, these models have been used for inverse problem solving [33] [14] and to understanding the latent representations of the distributions.

Diffusion Models Diffusion models, in particular, have been making huge improvements and have been used in many domains due to their high generative capabilities. There are mainly two types of diffusion models, one is the Score based approach introduced by Song and Ermon [32] and the other, which is the focus of this work, is the one introduced by Ho et al. [7]. Both modeling types have been able to achieve state-of-the-art performance in generative modeling tasks and have motivated the growth of many sub-

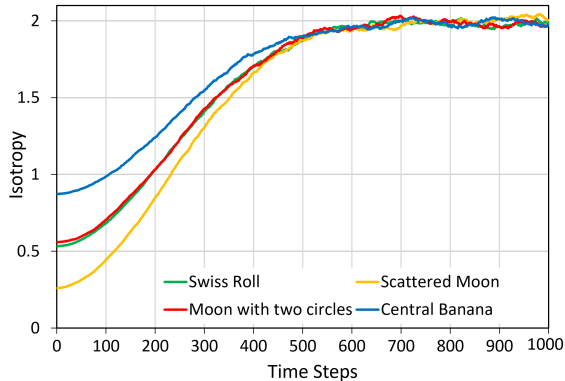


Figure 2. Variation of isotropy of the data distribution along the forward diffusion process for the 2D synthetic datasets. As can be seen from the plot, in the limit, the data distribution reaches the value of two, which happens to be the dimension of an isotropic random vector in \mathbb{R}^2 (expected squared norm of an isotropic random vector).

sequent works in generative models.

Improving Diffusion Models In the context of DDPMs [7], there have been several seminal papers that have contributed to the improvement of these models. In particular, Nichol et al.’s [19] work presented several key insights into how one could improve the training of these models. One such insight is the use of a cosine-based variance schedule rather than the linear variance schedule used by Ho et al. [7]. These changes were able to improve the DDPM further.

However, most of these improvements were focused on improving the models based on the most widely used metrics for image generation, FID and IS. But some of the recent work ([13], [16], [25]), in generative models has pointed out that FID and IS are not necessarily indicative of the actual fidelity of the samples generated by generative models. Thus, researchers have been focusing on finding other metrics, such as Precision and Density, to assess the fidelity of these generated samples [2], [30]. In particular, we observed that the Density takes the local context (measuring how close it is to densely packed samples of the true distribution) of a sample into account during its calculation. We believe that this makes the Density a vital metric to assess the samples’ fidelity.

3. Background

Diffusion probabilistic models were first introduced by Sohl-Dickstein et al. [31] These models fall under the category of generative models which learn the distribution of the data so that they can sample from these data distributions. However, it was not until Ho et al. [7] that Diffusion Probabilistic Models took off. In the next few subsections,

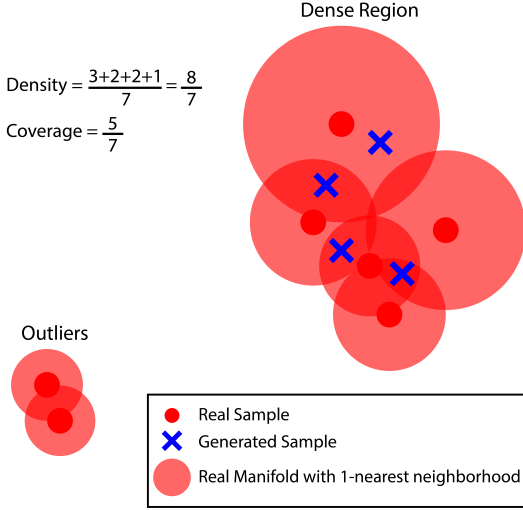


Figure 3. An example scenario for illustrating a situation where high Density and low Coverage is recorded. Generating samples in the neighborhoods of the highly dense regions over the outliers in the true manifold has resulted in a high Density and low Coverage.

we will provide a brief overview of the DDPM definitions that will be useful to understanding our work.

3.1. Definitions

In the DDPM, we simply add a Gaussian noise, which varies according to a specific variance schedule, $\beta_t \in (0, 1)$. The noise at each time-step corrupts the data, such that by the time the time-step reaches its final value, T , the data will be mapped to an almost isotropic Gaussian distribution. However, the learning occurs when we try to learn the reverse process by which we try to denoise along the same trajectory starting from the almost isotropic Gaussian distribution. The first process, in which we add noise, is called the forward process and the latter, in which we denoise, is called the reverse process. The forward process is often characterized by q and the reverse process by p . Both of which are modeled as Gaussian distributions.

The forward process is defined as follows,

$$q(x_1, x_2, \dots, x_T | x_0) = \prod_{t=1}^T q(x_t | x_{t-1}) \quad (1)$$

$$q(x_t | x_{t-1}) \sim \mathcal{N}(x_t; \sqrt{1 - \beta_t} x_{t-1}, \beta_t \mathbf{I}) \quad (2)$$

Moreover, by introducing $\alpha_t = 1 - \beta_t$ as well as $\bar{\alpha}_t = \prod_{i=1}^t \alpha_i$ the forward process can be further simplified into the following expression via the re-parametrization trick [11]. Since,

$$q(x_t | x_{t-1}) \sim \mathcal{N}(x_t; \sqrt{1 - \beta_t} x_{t-1}, \beta_t \mathbf{I}) \quad (3)$$

$$q(x_t | x_0) \sim \mathcal{N}(x_t; \sqrt{\bar{\alpha}_t} x_0, \sqrt{1 - \bar{\alpha}_t} \mathbf{I}) \quad (4)$$

$$x_t = \sqrt{\bar{\alpha}_t} x_0 + \sqrt{1 - \bar{\alpha}_t} \epsilon \quad (5)$$

where, $\epsilon \in \mathcal{N}(0, \mathbf{I})$.

The reverse process, given by $p \sim \mathcal{N}(x_{t-1} | x_t)$, can be obtained in terms of the forward process distribution q and Baye's Theorem. However, the reverse process only becomes tractable when the posterior distribution $q(x_{t-1} | x_t)$, is conditioned on the input data x_0 . Thus, during training, the model tries to learn the tractable $q(x_{t-1} | x_t, x_0)$ distribution. This distribution, which is also a Gaussian distribution, is defined by the following equation and parameters.

$$q(x_{t-1} | x_t, x_0) \sim \mathcal{N}(x_{t-1}; \tilde{\mu}(x_t, x_0), \tilde{\beta}_t \mathbf{I}) \quad (6)$$

$$\tilde{\beta}_t = \frac{1 - \bar{\alpha}_{t-1}}{1 - \bar{\alpha}_t} \beta_t \quad (7)$$

$$\tilde{\mu}_t(x_t, x_0) = \frac{\sqrt{\bar{\alpha}_{t-1}} \beta_t}{1 - \bar{\alpha}_t} x_0 + \frac{\sqrt{\bar{\alpha}_t} (1 - \bar{\alpha}_{t-1})}{1 - \bar{\alpha}_t} x_t \quad (8)$$

3.2. Training Process

To train, however, one could make the model predict the mean of the reverse process distribution at each time step. But Ho et al. [7] mentions that predicting the additive noise, ϵ , leads to better results. The additive noise and the mean of the reverse process distribution at each time step are elegantly linked by equations 5 and 8. This results in the following re-parametrization of $\tilde{\mu}(x_t, t)$,

$$\tilde{\mu}(x_t, t) = \frac{1}{\sqrt{\alpha_t}} \left(x_t - \frac{1 - \alpha_t}{\sqrt{1 - \bar{\alpha}_t}} \epsilon \right) \quad (9)$$

Therefore, predicting the additive noise ϵ , is adequate for the task of predicting the mean of the backward process distribution. Moreover, since the forward process' variance schedule is fixed, the reverse process variance, $\tilde{\beta}_t$, is also assumed to be fixed according to $\tilde{\beta}_t$.

Thus, Ho et al. [7] proposes to optimize the following simple objective function during the training process.

$$L_{\text{simple}} = E_{t, x_0, \epsilon} [|\epsilon - \epsilon_\theta(x_t, t)|^2] \quad (10)$$

where $\epsilon_\theta(x_t, t)$ is the predicted noise.

3.3. Hidden Statistical Properties of ϵ

As discussed earlier, one of the main objectives of the proposed algorithm is to identify a learnable isotropic measure that best reflects the overall isotropic nature of the learned samples. This will allow backpropagation to accurately guide the model toward the maximum isotropy at the vanishing point. The identified metric (11) is the expected squared norm of ϵ which will be named isotropy.

$$\text{Isotropy} = E(\epsilon^T \epsilon) \quad (11)$$

Upon closer inspection of the L_{simple} objective function, we see that the objective of the U-Net is to minimize the

mean squared error between ϵ and ϵ_θ . Yet, if the simple loss is expanded further, a rather informative mathematical expression can be obtained.

$$E[||\epsilon - \epsilon_\theta||^2] = E[(\epsilon - \epsilon_\theta)^T(\epsilon - \epsilon_\theta)] \quad (12)$$

$$= E(\epsilon^T \epsilon) + E(\epsilon_\theta^T \epsilon_\theta) - 2E(\epsilon_\theta^T \epsilon) \quad (13)$$

Now, since we know that $\epsilon \sim \mathcal{N}(0, \mathbf{I})$, it is an isotropic distribution. Thus, by definition, since ϵ is an isotropic random vector in \mathbb{R}^n , the expected norm of the random vector, $E(\epsilon^T \epsilon) = n$.

Furthermore, since the goal is to predict the noise as accurately as possible, ϵ_θ should also be distributed according to an isotropic Gaussian distribution, i.e., $\epsilon_\theta \sim \mathcal{N}(0, \mathbf{I})$. Hence, if ϵ and ϵ_θ are both identical isotropic random vectors,

$$E[||\epsilon - \epsilon_\theta||^2] = E(\epsilon^T \epsilon) + E(\epsilon_\theta^T \epsilon_\theta) - 2E(\epsilon_\theta^T \epsilon) \quad (14)$$

$$= n + n - 2n \quad (15)$$

$$= 0 \quad (16)$$

4. Analysis on the Isotropy of x_t

Based on the observations, we were inspired to find out further implications of imposing structural information in the DDPM. As it turns out, we were able to gain more interesting insights about the forward process of the DDPM. For example, if we consider equation 5 and consider the isotropy, expected squared norm of x_t , we see that,

$$\begin{aligned} E(||x_t||^2) &= E(x_t^T x_t) \\ &= \bar{\alpha}_t E(x_0^T x_0) + (1 - \bar{\alpha}_t) E(\epsilon^T \epsilon) \\ &\quad + 2\sqrt{\bar{\alpha}_t(1 - \bar{\alpha}_t)} E(x_0^T \epsilon) \end{aligned} \quad (17)$$

However, since ϵ is an isotropic Gaussian random vector, it is isotropic. Moreover, by assuming that it is independent of the distribution of x_0 , when x_0 is non-isotropic, we see that,

$$E(x_0^T \epsilon) = 0 \quad (18)$$

Therefore,

$$E(x_t^T x_t) = \bar{\alpha}_t E(x_0^T x_0) + (1 - \bar{\alpha}_t)n \quad (19)$$

$$= n + \bar{\alpha}_t(E(x_0^T x_0) - n) \quad (20)$$

Thus, when the input data are normalized and they are distributed according to a non-isotropic distribution, we note that the maximum of the expected squared norm of x_0 , $E(x_0^T x_0)_{\max} = n$. Hence, $E(x_0^T x_0) - n \leq 0$. Thus, during the forward process, since $\bar{\alpha}_t > 0$, the expected squared norm of x_t can be at most n , $\forall t \in [1, T]$ and attains the maximum value at the final time-step T .

$$E(x_t^T x_t) \leq n \quad (21)$$

Moreover, when we consider two consecutive time steps, t and $t + 1$, we see that,

$$E(x_{t+1}^T x_{t+1}) = n + \bar{\alpha}_{t+1}(E(x_0^T x_0) - n) \quad (22)$$

$$E(x_t^T x_t) = n + \bar{\alpha}_t(E(x_0^T x_0) - n) \quad (23)$$

$$E(x_{t+1}^T x_{t+1}) - E(x_t^T x_t) = (E(x_0^T x_0) - n)(\bar{\alpha}_{t+1} - \bar{\alpha}_t) \quad (24)$$

We know that $E(x_0^T x_0) - n \leq 0$ and that $\bar{\alpha}_{t+1} - \bar{\alpha}_t \leq 0$. Thus,

$$E(x_{t+1}^T x_{t+1}) - E(x_t^T x_t) \geq 0 \quad (25)$$

$$E(x_{t+1}^T x_{t+1}) \geq E(x_t^T x_t) \quad (26)$$

Therefore, for any particular normalized data distribution, we see that during the forward process, the isotropy of the data distribution increases. Finally, converges to the isotropy of an isotropic random Gaussian vector, when the data distribution completely converts into an isotropic Gaussian distribution (see Figure 2). Hence, the definition of isotropy given in this paper aligns perfectly with the fact that the isotropy quantifies structural information about the data distribution.

5. Isotropy Based Loss Function

In the default DDPM model, the variance schedule drives the transformation toward an isotropic Gaussian distribution by restricting the degrees of freedom for the movement of information of the distribution, without using backpropagation to adaptively learn the degree of isotropy achieved, making it, a non-learnable process. Armed with the above analyses, we proceeded to modify the objective function L_{simple} to include a regularization term which penalizes the model, if the model predicts a noise which is not necessarily isotropic. Hence, the new modified objective function we propose to optimize is,

$$L_{\text{modified}} = E(||\epsilon - \epsilon_\theta||^2) + \lambda(E(\epsilon_\theta^T \epsilon_\theta) - n)^2 \quad (27)$$

where λ is the regularization parameter.

However, this modified objective needs to be further simplified so as to make this new error, independent of the size of the dimension of the random vector. Thus, we make the following modification during implementation.

$$L_{\text{modified}} = E(||\epsilon - \epsilon_\theta||^2) + \lambda \left(E \left(\frac{\epsilon_\theta^T \epsilon_\theta}{n} \right) - 1 \right)^2 \quad (28)$$

6. Interpret the Evaluation Metrics

Precision denotes the fraction of generated data that lies in the true manifold, by counting whether each generated data

| Metrics | Swiss Roll | | Scattered Moon | | Moon with two circles | | Central Banana | |
|-----------|---------------|-------------------------|----------------|------------------------|-----------------------|------------------------|----------------|------------------------|
| | DDPM | Ours | DDPM | Ours | DDPM | Ours | DDPM | Ours |
| Precision | 0.9458 | 0.9893 (+4.60%) | 0.9990 | 0.9993 (+0.03%) | 0.9921 | 0.9982 (+0.61%) | 0.8974 | 0.9072 (+1.09%) |
| Recall | 0.9927 | 0.9709 (-2.19%) | 0.9962 | 0.9736 (-2.27%) | 0.9967 | 0.9694 (-2.74%) | 0.9977 | 0.9417 (-5.61%) |
| Density | 0.8946 | 0.9908 (+10.75%) | 1.0015 | 1.0049 (+0.34%) | 0.9925 | 1.0081 (+1.57%) | 0.8785 | 0.8962 (+2.01%) |
| Coverage | 0.8932 | 0.8458 (-5.31%) | 0.9605 | 0.8254 (-14.07%) | 0.9498 | 0.8572 (-9.75%) | 0.9102 | 0.6840 (-24.85%) |

Table 1. Comparison of Evaluation Metrics for the two methods: DDPM and Iso-Diffusion for the 2D Datasets

| Metrics | Oxford Flower | | Oxford-IIIT-Pet | | CIFAR-10 | | CIFAR-100 | |
|--------------------------|---------------|-------------------------|-----------------|-------------------------|--------------|------------------------|--------------|-----------------------|
| | DDPM | Ours | DDPM | Ours | DDPM | Ours | DDPM | Ours |
| FID (\downarrow) | 55.590 | 47.310 (-14.9%) | 34.087 | 31.900 (-6.4%) | 16.023 | 11.872 (-25.9%) | 14.794 | 14.141 (-4.4%) |
| IS (\uparrow) | 3.097 | 3.504 (+13.1%) | 7.083 | 7.531 (+6.3%) | 8.463 | 8.482 (+0.2%) | 9.032 | 9.183 (+1.7%) |
| Precision (\uparrow) | 0.725 | 0.944 (+30.3%) | 0.819 | 0.954 (+16.5%) | 0.607 | 0.689 (+13.6%) | 0.638 | 0.710 (+11.4%) |
| Recall (\uparrow) | 0.184 | 0.056 (-69.8%) | 0.152 | 0.063 (-58.4%) | 0.447 | 0.384 (-14.0%) | 0.398 | 0.350 (-12.1%) |
| Density (\uparrow) | 2.632 | 11.039 (+319.4%) | 6.704 | 15.778 (+135.4%) | 1.401 | 2.104 (+50.3%) | 1.479 | 2.190 (+48.1%) |
| Coverage (\uparrow) | 0.959 | 0.994 (+3.6%) | 0.9996 | 0.9999 (+0.03%) | 0.987 | 0.995 (+0.8%) | 0.9996 | 0.9996 (0.0%) |

Table 2. Comparison of Evaluation Metrics for the two methods: DDPM and Iso-Diffusion for the Image Datasets.

point falls within a neighborhood sphere of real samples. This measure reflects how closely the generated points align with the true manifold [13], [27].

Recall denotes the fraction of true data that lies in the generated manifold, by counting whether each true data point falls within a neighborhood sphere of generated samples. This measure indicates how well the true points align with the generated manifold [13], [27].

Density counts the number of neighborhood spheres of real samples that encompass each generated data point. This allows Density to reward generated samples located in areas densely populated by real samples, reducing sensitivity to outliers. This enables to consider the local context of a distribution by measuring how close a sample is to densely packed points in the true distribution [16].

Coverage measures the fraction of real samples whose neighborhoods contain at least one generated sample. Moreover, Coverage measures the diversity of a distribution by assessing whether all aspects of the distribution are represented. However, the presence of sparse outliers in the true manifold and the absence of the generated samples near those outliers may result in low Coverage [16]. (see Figure 3)

7. Experiments

7.1. Experimental Setup

To validate our approach we consider 2D synthetic data as well as images. For the 2D data, we utilized a conditional dense network consisting of 3 fully-connected hidden layers with ReLU activations. The learning rate was fixed

at $1e-3$. All the datasets were learned using 1000 time-steps and 1000 epochs. For the image datasets, we consider the same version of the U-Net utilized in the original DDPM implementation with a learning rate of $2e-4$. The U-Net training involved 1000 time-steps and 1000 epochs for the Oxford Flower and Oxford-IIIT Pet datasets, while the CIFAR-10 and CIFAR-100 datasets were trained with 2000 epochs. Metrics are reported as the average of 3 training runs per dataset, with PRDC values calculated using $k=5$ nearest neighbors for each dataset. Moreover, all the experiments were run on one Quadro GV-100 GPU with 32GB of VRAM.

7.2. Performance comparison between DDPM and Iso-Diffusion

To compare the performance between DDPM and Iso-Diffusion, the modified loss function was utilized in all four 2D synthetic datasets, Oxford Flower dataset, Oxford IIIT Pet dataset and CIFAR-10 dataset. Precision, Recall, Density along with Coverage were used to evaluate and compare the performance of the two models on 2D synthetic datasets. In addition to those four evaluation metrics, FID and IS were used to evaluate the quality of the generated samples for the image datasets Oxford Flower, Oxford-IIIT Pet, CIFAR-10 and CIFAR-100.

Table 1 demonstrates the comparison between the best performing isotropy based model (Iso-Diffusion) and DDPM in terms of the generative model’s evaluation metrics along with the percentage change from DDPM. Across all these 2D synthetic datasets we observed that the fidelity metrics, Precision and Density have been improved in Iso-

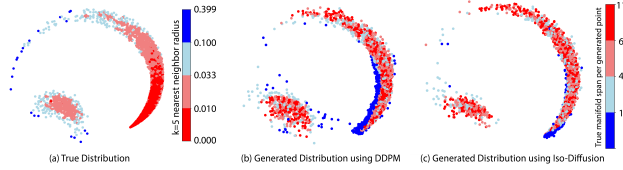


Figure 4. Center Banana 2D synthetic dataset. (a) True distribution points, color-coded by $k=5$ nearest neighbor radius. (b) DDPM-generated points, color-coded by true manifold span per point. (c) Iso-Diffusion generated points, color-coded by true manifold span per point.

Diffusion. The results of Table 2 further confirm the improvements made by our modified loss on the quality of image samples. The Density of the generated images has been significantly improved for all four datasets. Moreover, the FID score has been significantly improved in the CIFAR-10 dataset by the proposed method.

Although the performance of the modified loss function has been able to produce sample which surpass the original DDPM’s samples quality, the quality depends on the regularization parameter of the modified loss function. In particular, we performed a few more experiments by considering a range of values for the regularization parameter. The metrics for the Oxford Flower dataset and Oxford-IIIT-Pet dataset with different values of the regularization parameter ranging from 0.01 to 0.30 are tabulated in Table 3 and Table 4. We see that the fidelity metrics, Precision and Density, gradually improve with the increase of the regularization parameter. However, we can see that the diversity metrics, Recall and Coverage, gradually decline with the parameter.

Although the FID and IS are considered to be the most widely used evaluation metrics for assessing image generation, we see that in the case of all four datasets, they convey little to no discerning information about the generative ability of the proposed method and the original DDPM. But, by using other metrics such as the Precision, Recall, Density and Coverage, we can state that while our proposed method suffers a bit in terms of Recall, the generated samples, are very close to being real (see Figure 1), as indicated by the improvements in the Precision and Density metrics.

7.3. Interpretation of the results of 2D data distributions using PRDC values

We believe that the disparity in the changes of Precision, Recall, Density and Coverage is a direct consequence of imposing a structural constraint on the objective function. It is evident that by focusing on the structure or the isotropy of the distribution, our method is capable of capturing highly dense mode regions and generating samples near them rather than being too diverse. Thus, it increases the fidelity but decreases the diversity of the generated samples.

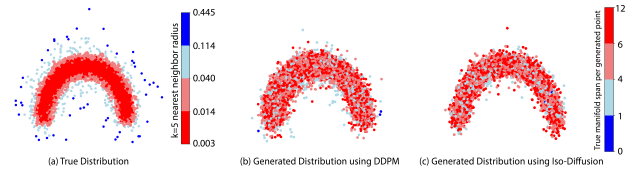


Figure 5. Scattered Moon 2D synthetic dataset. (a) True distribution points, color-coded by $k=5$ nearest neighbor radius. (b) DDPM-generated points, color-coded by true manifold span per point. (c) Iso-Diffusion generated points, color-coded by true manifold span per point.

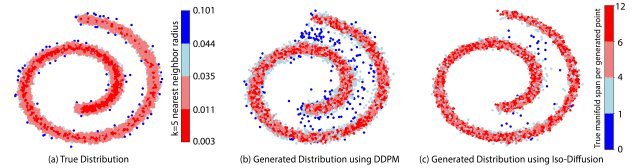


Figure 6. Swiss Roll 2D synthetic dataset. (a) True distribution points, color-coded by $k=5$ nearest neighbor radius. (b) DDPM-generated points, color-coded by true manifold span per point. (c) Iso-Diffusion generated points, color-coded by true manifold span per point.

As illustrated in the Figure 4(a), the Central Banana distribution was designed by introducing a distinct mode to the main structure of the distribution resulting in a multimodal distribution with a density gradient. Once, it is generated via Iso-Diffusion as indicated in Figure 4(c), it is evident that, Iso-Diffusion, is capable of capturing the main structure even with the discontinuities of the density gradient. However, the illustrations show that DDPM lacks the capability of capturing the discontinuity in the density gradient between the tail end of the main distribution and the distinct mode. Instead, it tries to generate data points that are actually not even in the true distribution by interpolating along the main lobe’s trend (see Figure 4(b)). Moreover, the limited capability to capture the discontinuity in the density gradient of DDPM can be further observed in the Swiss Roll distribution as well (see Figure 6(b) and 6(c)). The increase in Density and decrease in Coverage for the datasets Swiss Roll and Central Banana are clear evidence for the aforementioned observations. Hence, it is limited in ability to capture the underlying structure of the distribution. Additionally, there is a noticeable trend of generating data points (blue points in Figure 4(b), 4(c)), outside the boundaries of the highly dense regions of the main lobe. This effect is likely due to the model’s focus on these high-density regions. However, compared to DDPM, Iso-Diffusion effectively regulates the overgeneration of data points outside the boundaries of densely packed regions. This improvement is likely a result of the added regularization in the improved

| Method | FID (\downarrow) | IS (\uparrow) | Precision (\uparrow) | Recall (\uparrow) | Density (\uparrow) | Coverage (\uparrow) |
|-----------------------|----------------------|-------------------|--------------------------|-----------------------|------------------------|-------------------------|
| DDPM | 55.5900 | 3.0970 | 0.7248 | 0.1840 | 2.6320 | 0.9588 |
| Ours $\lambda = 0.01$ | 53.3374 | 3.2023 | 0.7839 | 0.1570 | 3.3445 | 0.9758 |
| Ours $\lambda = 0.05$ | 54.7064 | 3.2208 | 0.733 | 0.17625 | 2.6384 | 0.9586 |
| Ours $\lambda = 0.10$ | 47.3097 | 3.5037 | 0.9441 | 0.0555 | 11.0389 | 0.9935 |
| Ours $\lambda = 0.30$ | 51.5820 | 3.3105 | 0.9460 | 0.0549 | 12.5441 | 0.9946 |

Table 3. Metrics Variation with the Regularization Parameter for the Oxford Flower Dataset (λ)

| Method | FID (\downarrow) | IS (\uparrow) | Precision (\uparrow) | Recall (\uparrow) | Density (\uparrow) | Coverage (\uparrow) |
|-----------------------|----------------------|-------------------|--------------------------|-----------------------|------------------------|-------------------------|
| DDPM | 34.0874 | 7.0827 | 0.8189 | 0.1522 | 6.7040 | 0.9996 |
| Ours $\lambda = 0.01$ | 32.7278 | 7.5298 | 0.8805 | 0.1233 | 7.9743 | 0.9991 |
| Ours $\lambda = 0.05$ | 32.4877 | 7.5156 | 0.8628 | 0.1263 | 8.0348 | 0.9997 |
| Ours $\lambda = 0.10$ | 33.3405 | 7.4813 | 0.9103 | 0.1015 | 10.6351 | 1.0000 |
| Ours $\lambda = 0.30$ | 31.8998 | 7.5313 | 0.9542 | 0.0633 | 15.7780 | 0.9999 |

Table 4. Metrics Variation with the Regularization Parameter for the Oxford-IIIT-Pet Dataset (λ)

object function, which encourages capturing the main semantics of the true distribution.

As illustrated in the Figure 5(a), the Scattered Moon distribution was designed by imposing scattered noise around the main structure of the data distribution. Once, it is generated via Iso-Diffusion as indicated in the Figure 5(c), it is evident that, the model has tried to only capture the underlying semantics of the distribution without being susceptible to the low probable regions. Whereas, the DDPM model shows limitations in capturing the distinction between the main structure and the scattered noise (see Figure 5(b)). The increased Density and reduced Coverage values support this observation. This shows that the proposed objective function, enforces the generated samples to contain properties that push them to be closely linked to the real data. Thus, we can directly observe an improvement in the Density metric as it measures the sample fidelity. We believe that in the context of unconditional image generation, the isotropy based objective function helps the U-Net learn to keep the generated samples closer to the high-density regions of the ground-truth distribution.

These observations highlight the proposed algorithm’s ability to increase Density by focusing on the dense regions of the true distribution. At the same time, the absence of generated data in the neighborhoods of low probable data points in the true distribution may result in a reduction in Coverage. When scattering is minimal, Coverage remains consistent. This indicates that the algorithm effectively captures the main structure of the true distribution without extending into low probable regions. Also, each of these metrics has their own utility depending on the application [13]. Thus, this should motivate the research community to propose new evaluation metrics such as Density, which is a much more meaningful measure of fidelity over FID and

IS, to assess generative models.

Preserving the modality of a data distribution is essential, as failing to capture it can lead to a loss of semantic details or edge information, both of which represent high-level features in computer vision and image processing tasks [4], [29]

8. Conclusion

Denosing Diffusion Probabilistic Models have achieved state-of-the-art performance in generative modeling tasks such as unconditional image generation and image super-resolution. However, these models can still be improved upon and much work has been put into improving them. In this paper, we propose another improvement method that is built on the premise that since the distribution that the forward process terminates and the reverse process initiates at an isotropic Gaussian distribution, which is void of any structure, it is well motivated, that the incorporation of isotropy as a measure of structure on the loss function will improve the DDPMs’ generated sample fidelity. We, theoretically, show that isotropy is well a defined metric to measure the structure of the distribution during the forward process and the proposed modification helps the DDPM to converge to better solutions based on the simple modified loss. We show that the Iso-Diffusion objective function regulates data point generation, aligning it with the prominent structures of the true distribution and anchoring the process to dense, information-rich modes. Finally, we validate and show that our modified objective function improves DDPM performance through experiments on 2D synthetic datasets and unconditional image generation, supported by an in-depth analysis and evidenced by improved fidelity and diversity metrics.

References

- [1] Prafulla Dhariwal and Alex Nichol. Diffusion models beat gans on image synthesis, 2021. 1
- [2] Nicolas Dufour, Victor Besnier, Vicky Kalogeiton, and David Picard. Don't drop your samples! coherence-aware training benefits conditional diffusion. In *2024 IEEE/CVF Conference on Computer Vision and Pattern Recognition (CVPR)*, pages 6264–6273, 2024. 3
- [3] Ian Goodfellow, Jean Pouget-Abadie, Mehdi Mirza, Bing Xu, David Warde-Farley, Sherjil Ozair, Aaron Courville, and Yoshua Bengio. Generative adversarial networks. *Communications of the ACM*, 63(11):139–144, 2020. 3
- [4] Senhui Guo, Jing Xu, Dapeng Chen, Chao Zhang, Xiaogang Wang, and Rui Zhao. Density-aware feature embedding for face clustering. In *2020 IEEE/CVF Conference on Computer Vision and Pattern Recognition (CVPR)*, pages 6697–6705, 2020. 8
- [5] Martin Heusel, Hubert Ramsauer, Thomas Unterthiner, Bernhard Nessler, and Sepp Hochreiter. Gans trained by a two time-scale update rule converge to a local nash equilibrium. *Advances in neural information processing systems*, 30, 2017. 2
- [6] Jonathan Ho and Tim Salimans. Classifier-free diffusion guidance. *arXiv preprint arXiv:2207.12598*, 2022. 1
- [7] Jonathan Ho, Ajay Jain, and Pieter Abbeel. Denoising diffusion probabilistic models. *Advances in neural information processing systems*, 33:6840–6851, 2020. 1, 3, 4
- [8] Jonathan Ho, William Chan, Chitwan Saharia, Jay Whang, Ruiqi Gao, Alexey Gritsenko, Diederik P Kingma, Ben Poole, Mohammad Norouzi, David J Fleet, et al. Imagen video: High definition video generation with diffusion models. *arXiv preprint arXiv:2210.02303*, 2022. 3
- [9] Jonathan Ho, Chitwan Saharia, William Chan, David J Fleet, Mohammad Norouzi, and Tim Salimans. Cascaded diffusion models for high fidelity image generation. *The Journal of Machine Learning Research*, 23(1):2249–2281, 2022. 1
- [10] Jaeseok Jeong, Mingi Kwon, and Youngjung Uh. Training-free content injection using h-space in diffusion models, 2024. 1
- [11] Diederik P Kingma and Max Welling. Auto-encoding variational bayes. *arXiv preprint arXiv:1312.6114*, 2013. 3, 4
- [12] Alex Krizhevsky, Vinod Nair, and Geoffrey Hinton. Cifar-10 (canadian institute for advanced research). 2
- [13] Tuomas Kynkäänniemi, Tero Karras, Samuli Laine, Jaakko Lehtinen, and Timo Aila. Improved precision and recall metric for assessing generative models. *Advances in Neural Information Processing Systems*, 32, 2019. 1, 2, 3, 6, 8
- [14] Charles Laroche, Andrés Almansa, and Eva Coupete. Fast diffusion em: a diffusion model for blind inverse problems with application to deconvolution, 2023. 3
- [15] Shentong Mo, Enze Xie, Yue Wu, Junsong Chen, Matthias Nießner, and Zhenguo Li. Fast training of diffusion transformer with extreme masking for 3d point clouds generation. 2023. 3
- [16] Muhammad Ferjad Naeem, Seong Joon Oh, Youngjung Uh, Yunjey Choi, and Jaejun Yoo. Reliable fidelity and diversity metrics for generative models. 2020. 1, 2, 3, 6
- [17] Alex Nichol and Prafulla Dhariwal. Improved denoising diffusion probabilistic models, 2021. 1
- [18] Alex Nichol, Prafulla Dhariwal, Aditya Ramesh, Pranav Shyam, Pamela Mishkin, Bob McGrew, Ilya Sutskever, and Mark Chen. Glide: Towards photorealistic image generation and editing with text-guided diffusion models. *arXiv preprint arXiv:2112.10741*, 2021. 1
- [19] Alexander Quinn Nichol and Prafulla Dhariwal. Improved denoising diffusion probabilistic models. In *International Conference on Machine Learning*, pages 8162–8171. PMLR, 2021. 1, 3
- [20] Maria-Elena Nilsback and Andrew Zisserman. Automated flower classification over a large number of classes. In *2008 Sixth Indian conference on computer vision, graphics & image processing*, pages 722–729. IEEE, 2008. 2
- [21] Omkar M. Parkhi, Andrea Vedaldi, Andrew Zisserman, and C. V. Jawahar. Cats and dogs. In *IEEE Conference on Computer Vision and Pattern Recognition*, 2012. 2
- [22] Aditya Ramesh, Prafulla Dhariwal, Alex Nichol, Casey Chu, and Mark Chen. Hierarchical text-conditional image generation with clip latents. *arXiv preprint arXiv:2204.06125*, 1(2):3, 2022. 1
- [23] Danilo Rezende and Shakir Mohamed. Variational inference with normalizing flows. In *International conference on machine learning*, pages 1530–1538. PMLR, 2015. 3
- [24] Robin Rombach, Andreas Blattmann, Dominik Lorenz, Patrick Esser, and Björn Ommer. High-resolution image synthesis with latent diffusion models. In *Proceedings of the IEEE/CVF conference on computer vision and pattern recognition*, pages 10684–10695, 2022. 1
- [25] Andrea Rosasco, Stefano Berti, Giulia Pasquale, Damiano Malafronte, Shogo Sato, Hiroyuki Segawa, Tetsugo Inada, and Lorenzo Natale. Concon-chi: Concept-context chimera benchmark for personalized vision-language tasks. In *2024 IEEE/CVF Conference on Computer Vision and Pattern Recognition (CVPR)*, pages 22239–22248, 2024. 3
- [26] Chitwan Saharia, William Chan, Saurabh Saxena, Lala Li, Jay Whang, Emily L Denton, Kamyar Ghasemipour, Raphael Gontijo Lopes, Burcu Karagol Ayan, Tim Salimans, et al. Photorealistic text-to-image diffusion models with deep language understanding. *Advances in Neural Information Processing Systems*, 35:36479–36494, 2022. 1
- [27] Mehdi S. M. Sajjadi, Olivier Bachem, Mario Lucic, Olivier Bousquet, and Sylvain Gelly. Assessing generative models via precision and recall, 2018. 6
- [28] Tim Salimans, Ian Goodfellow, Wojciech Zaremba, Vicki Cheung, Alec Radford, and Xi Chen. Improved techniques for training gans. *Advances in neural information processing systems*, 29, 2016. 2
- [29] Tamar Rott Shaham, Tali Dekel, and Tomer Michaeli. Singan: Learning a generative model from a single natural image. In *Proceedings of the IEEE/CVF International Conference on Computer Vision (ICCV)*, 2019. 8
- [30] Jaisidh Singh, Harshil Bhatia, Mayank Vatsa, Richa Singh, and Aparna Bharati. Synthprov: Interpretable framework for profiling identity leakage. In *2024 IEEE/CVF Winter Conference on Applications of Computer Vision (WACV)*, pages 4734–4744, 2024. 3

- [31] Jascha Sohl-Dickstein, Eric Weiss, Niru Maheswaranathan, and Surya Ganguli. Deep unsupervised learning using nonequilibrium thermodynamics. In *International conference on machine learning*, pages 2256–2265. PMLR, 2015. [3](#)
- [32] Yang Song and Stefano Ermon. Generative modeling by estimating gradients of the data distribution. *Advances in neural information processing systems*, 32, 2019. [3](#)
- [33] Yang Song, Liyue Shen, Lei Xing, and Stefano Ermon. Solving inverse problems in medical imaging with score-based generative models. *arXiv preprint arXiv:2111.08005*, 2021. [3](#)
- [34] Roman Vershynin. *High-dimensional probability: An introduction with applications in data science*. Cambridge university press, 2018. [2](#)